DATA REPOSITORY SECTION 1. PHOTOGRAPHS OF CENOZOIC STRATA

Lithofacies 1, 1a, 2, and 3 are shown in Figure A1.

DATA REPOSITORY SECTION 2. PRE-CENOZOIC BASIN FILL

Facies J1-grey slate pebble conglomerate interbedded with red mudstone- Discontinuous outcrops of facies 1 floor the basin near the town of Yangqu (Figs. 2, 3). Facies J1 consists of dark red mudstone with grey lenses of pebble conglomerate. The conglomerate lenses exhibit angular-subangular slate clasts, and a quartz sand matrix. They display imbrication, and they are typically clast supported. The beds contain small, silty or fine sand lenses, that are ~3-4 centimeters thick and a 10 – 30 centimeters wide. Near the base of the unit, gravel lenses are 2-15 centimeters thick and laterally continuous over 1 – 3 meters. Upsection, the gravel beds amalgamate. The mudstone comprises silty clay, and the beds appear to be internally structureless. Beds are laterally continuous, 10 – 30 centimeters thick, and the sand lenses are inset into the muddy matrix. Although most of the beds are dark red, near the base of the unit, mud beds may be grey, buff or red.

The imbricated clasts within this unit are interpreted to be traction deposits. The lenticular geometry of the gravel beds indicates that facies J1 was deposited by a channelized flow. The red color of the mudstone may indicate subaerial exposure of muddy units, if the oxidation of the sediments is a primary feature. We interpret the beds to be fluvial-floodplain deposits, such that the gravel lenses are channel deposits and the mud beds are overbank deposits.

Facies J2-grey, greenish grey, red and buff banded mudstone- Facies 2 sits conformably atop facies J1. Like facies J1, it only outcrops in discontinuous patches in the southern part of

Gonghe basin, near the town of Yangqu (Figs. 2, 3). Facies J2 consists of bands of grey, greenish grey, tan, brown and maroon silty clay mudstone, interbedded with a few lenses of buff colored, fine-medium sandstone. The mud beds are tabular, and laterally continuous. Each is a few tens of centimeters to a few meters thick. They exhibit maroon or orange mottling. One ~0.8 m thick coal bed is present. Sandstone lenses exhibit planar parallel laminations, trough cross stratification and planar cross stratification. Sandstone beds are 0.1 – 0.5 m thick, and laterally continuous over tens of meters.

The fine grain size and lack of sedimentary structures of facies J2 indicate deposition in relatively still water. The green and grey color of the many of the muds suggests subaqueous deposition. The red muds suggest periods of subaerial exposure. Trough cross-stratification and lenticular geometry of the sandstone lenses indicates that they were deposited by a unidirectional, laterally confined current. We interpret these to be interbedded fluvial (red muds, sandstones lenses) and lacustrine (grey green massive muds) deposits.

In order to develop a chronology for J1 and J2 deposits, we collected pollen samples from a coal bed at the base of J2 deposits, found 74 m above the basin floor, and about 100 m below the Cenozoic section. The bed contains a rich, well-preserved pollen assemblage, with a relatively low diversity of species. Although many of the species are long-ranging, from the Jurassic to the Cretaceous, the abundant *Corollinas* and *Quadraeculina anellaeformis* indicate the basal deposits are Early Jurassic in age. The coordinates of the pollen sample site are 35.70496° N, 100.16672° E, 3099 m.

DATA REPOSITORY SECTION 3. COSMOGENIC BURIAL AGE DATING

Field methods

To constrain the burial age of fluvial sediment from the Tongde basin, we collected 5 new samples of coarse fluvial sand or gravel for analysis of in-situ, cosmogenically produced ^{26}Al and ^{10}Be inventories in quartz (Granger and Muzikar, 2001; Granger, 2006). 4 of these samples were derived from the Yellow River canyon immediately north of the Gonghe Nan Shan (sample locations shown in Figs. 2, A2, A3), and a 5th was collected ~20 km north of the range (Fig. 2). Because the concentrations of cosmogenic ^{26}Al and ^{10}Be are strongly dependent on the history of post-burial muogenic isotope production within ~10 m of the earth's surface, we targeted samples from the base of modern roadcuts (Fig. A2), where we are able to geometrically constrain sample depth prior to historic road construction. Sampled roadcut exposures are unweathered and clearly exhibit original sedimentary structures of the basin fill. As a result, we are confident that the samples remained in-situ since the time of their deposition and were only recently exposed in the roadcuts.

Laboratory techniques

Samples were subjected to several physical and chemical treatments designed to purify the raw material to pure quartz. First, samples were crushed and sieved, in order to obtain a desirable grain size for the remaining treatments. In order to remove carbonates and minor metals, the crushed material was leached in nitric acid and aqua regia. Next, the sample was subjected to a suite of physical separation steps which were: froth flotation, magnetic separation, and following a purification bath in a hydrofluoric acid/nitric acid solution, heavy liquid separation. The remaining material was soaked for a second time in a hydrofluoric acid/nitric acid solution to remove any remaining feldspars. During this step, the outermost layers of the quartz grains were dissolved to remove meteoric ^{10}Be. After completing this routine, Al concentrations were measured on an inductively coupled plasma optical emissions spectrometer

(ICP-OES) to assess the purity of the remaining quartz. If the measured Al concentration (which signifies the presence of residual feldspars) exceeded 200 ppm, the final step was repeated as necessary.

In order to extract Be and Al isotopes from the purified quartz samples, a second series of chemical treatments was applied. After adding Be and Al carriers, quartz was dissolved in concentrated hydrofluoric acid. Following dissolution, an Al aliquot was extracted from the solution and prepared for precise measurement on the ICP-OES. The volume of the solution containing the dissolved sample was reduced and the hydrofluoric acid was removed by a series evaporation and fuming steps. The residual material was taken up in a sodium hydroxide solution, centrifuged, and decanted in order to separate Fe and Ti ions from the solid residual sample. Next the pH of the remaining solution was adjusted to ~8 to precipitate the Al and Be out of the solution as hydroxides (Ochs and Ivy-Ochs, 1997). After dissolving the remaining hydroxides in oxalic acid, cation and anion columns were used to removed residual Na, Fe, and other undesired ions, and to isolate Be and Al. The samples were dried and fired in an oven, and then loaded into a cathode for accelerator mass spectrometry (AMS). AMS was conducted at PRIME lab at Purdue University, following standard protocols.

Modeling of burial ages

For buried sediment that is derived from a steadily eroding source, the concentrations of unstable cosmogenic isotopes (in this case, ^{26}Al and ^{10}Be) will evolve through time as a function of two unknown variables, the pre-burial cosmogenic inventory and the time since burial (Granger and Muzikar, 2001).

$$(1) N_{Al}(t) = N_{Al}(0)\mathrm{e}^{(-t/\tau_{Al})} + P_{Al}(d)\tau_{Al}(1 - \mathrm{e}^{-t/\tau_{Al}})$$

$$(2) N_{Be}(t) = N_{Be}(0)\mathrm{e}^{(-t/\tau_{Be})} + P_{Be}(d)\tau_{Be}(1 - \mathrm{e}^{-t/\tau_{Be}})$$

where N_{Al} is the number of ^{26}Al atoms gram^{-1} of quartz, N_{Be} is the number ^{10}Be atoms gram^{-1} of quartz, t is time in years, P_{Al} is production rate of cosmogenic ^{26}Al in atoms year $^{-1}$gram^{-1}of quartz, P_{Be} is the production rate of cosmogenic ^{10}Be in atoms year^{-1} gram^{-1} of quartz, d is depth in cm, τ_{Al} is the radioactive mean-life of ^{26}Al (1.02 * 10^{6}yr) (Norris et al., 1983), and τ_{Be} is the radioactive mean-life of ^{10}Be (1.93 * 10^{6}yr) (Nishiizumi et al., 2007). The first term on the right hand side of (1) and (2) describes the post-burial decay of the isotopes and the second term describes the post-burial production of cosmogenic isotopes. For sediment that is buried to a sufficient depth, a few tens of meters, the second terms in (1) and (2) may be considered negligible, however, post-burial production significantly contributes to the inventory of cosmogenic isotopes in shallowly buried sediment (Granger and Smith, 2000; Granger and Muzikar, 2001; Wolkowinsky and Granger, 2004).

Under the assumption that a sample acquired its pre-burial inventory of cosmogenic isotopes as it was advected to the surface of a steadily eroding landscape, the initial concentration of a given cosmogenic isotope will simply be a function of the erosion rate.

$$(3) N_{Al}(0) = \frac{A_0}{\frac{1}{\tau_{Al}} + \frac{E}{L_0}} + \frac{A_1}{\frac{1}{\tau_{Al}} + \frac{E}{L_1}} + \frac{A_2}{\frac{1}{\tau_{Al}} + \frac{E}{L_2}} + \frac{A_3}{\frac{1}{\tau_{Al}} + \frac{E}{L_3}}$$

$$(4) N_{Be}(0) = \frac{B_0}{\frac{1}{\tau_{Be}} + \frac{E}{L_0}} + \frac{B_1}{\frac{1}{\tau_{Be}} + \frac{E}{L_1}} + \frac{B_2}{\frac{1}{\tau_{Be}} + \frac{E}{L_2}} + \frac{B_3}{\frac{1}{\tau_{Be}} + \frac{E}{L_3}}$$

Where E is erosion rate (cm yr^{-1}) and L_j refers to the attenuation length for a cosmogenic isotope production reaction (cm g cm^{-3}). L_0 is the attenuation length for spallogenic production reactions; L_1 and L_2 are the attenuation lengths for negative muon capture production reactions; and L_3 is the attenuation length for fast muon production reactions. We assign values of $L_0 = 160/\rho$, $L_1 = 738/\rho$, $L_2 = 2688/\rho$, and $L_3 = 4360/\rho$, where ρ is the density of the rock covering the sample in g cm^{-3} (Granger and Muzikar, 2001). We assume that prior to erosion, the target minerals were covered by rocks with a density of 2.6 g cm^{-3} (equations 3 and 4), and after burial, the target minerals were covered by sediment with a density of 2.0 g cm^{-3} (equations 5 and 6). The other constants, A_j and B_j, describe production rates for the various production reactions and have units of atoms year^{-1} gram^{-1} of quartz. We assign sea level high latitude values of $A_0 = 30$, $A_1 = 0.72$. $A_2 = 0.16$, $A_3 = 0.19$ (Granger and Muzikar, 2001 and references therein), such that the integrated sea level high latitude production rate of ^{26}Al is 31.07 atoms year^{-1} gram^{-1} of quartz. Previous investigators have estimated that the various production rate coefficients for ^{10}Be are $B_0 = 5$, $B_1 = 0.09$, $B_2 = 0.02$, and $B_3 = 0.02$ (Granger and Muzikar, 2001, and references therein). In aggregate, these values suggest a sea level high latitude ^{10}Be production rate of 5.13 atoms year^{-1} gram^{-1} of quartz. However, recent revision to the mean life of ^{10}Be (Nishiizumi et al., 2007), suggests that the production rate is slightly less, ~4.76 atoms year^{-1} gram^{-1} of quartz. Following this revision, we scale each of the ^{10}Be production rate coefficients by a factor of 4.76/5.13 so that the aggregate production rate conforms to the more recent value. As such, we use ^{10}Be coefficients of $B_0 = 4.64$, $B_1 = 0.08$, $B_2 = 0.02$, and $B_3 = 0.02$. This adjustment primarily affects the spallogenic production rate, B_0, and has little to no effect on the various muon production reaction rates. The values of A_j and B_j, were scaled to the field area using a latitude and altitude dependent correction for spallogenic production, and an atmospheric pressure dependent correction for all muogenic production reactions (Stone, 2000). We note that the production rates and atmospheric pressure scaling for fast muon reactions remain uncertain (Braucher et al., 2003; Wolkowinsky and Granger, 2004), but because the fast muon terms are small, we neglect any uncertainty that they introduce into our calculations.

For sediment that has not been buried to a sufficient depth to be completely shielded from cosmogenic radiation, post-burial production is described by the following relationships:

$$(5) P_{Al}(d) = A_0 \mathrm{e}^{-d/L_0} + A_1 \mathrm{e}^{-d/L_1} + A_2 \mathrm{e}^{-d/L_2} + A_3 \mathrm{e}^{-d/L_3}$$

$$(6) P_{Be}(d) = B_0 \mathrm{e}^{-d/L_0} + B_1 \mathrm{e}^{-d/L_1} + B_2 \mathrm{e}^{-d/L_2} + B_3 \mathrm{e}^{-d/L_3}$$

If the present day concentration of ^{26}Al and ^{10}Be is measured, and the burial depth is measured, then equations (1)-(6) can be combined to form a system of two equations with two unknowns, t and E. The equations may be solved graphically, or numerically. We present a graphical solution for these equations in Figure 6, but in practice, we have solved the equations numerically. This was done by forward modeling the range of possible combinations of t and E , and then identifying the t and E pair that best reproduces the modern day ^{26}Al/^{10}Be ratio and ^{10}Be concentration in a least squares sense (Fig. A4). We report 1σ uncertainties on each burial age.

Our calculations rely on three simplifying assumptions. First, we scale production rates of ^{26}Al and ^{10}Be to the sea level high latitude values using the present-day latitude and altitude of the samples. Because the quartz sand in each of the samples was eroded in a different location than it was deposited, this assumption introduces some error into our calculations. Second, we assume that analytical uncertainties on the concentrations of ^{26}Al and ^{10}Be encompass any uncertainties in the production rates and mean-lives of the isotopes. Third, we assume that post-burial muogenic isotope production is best calculated on the basis of the stratigraphic depth of each sample. Due to the fact that basin excavation appears to be recent and gradual, initiating at ~0.5 Ma and proceeding at vertical incision rates of ~100 m/Ma (Craddock et al., 2010), we make the simplifying assumption that post-excavation muogenic production along the evolving hillslope does not contribute significantly to measured cosmogenic inventories (c.f., Davis et al., 2011). This assumption should be particularly robust for samples with relatively high stratigraphic depths, because they were exhumed relatively recently. Moreover, vertical incision rates do not capture rates of canyon widening via retreat of angle of repose hillslopes and are likely to overestimate the rate at which our samples were excavated to shallow, pre-roadcut configurations. Recent application of burial age dating to correlative L3 deposits in central Tongde basin provides some evidence that our third assumption is reasonable (Craddock et al., 2010). Consideration of various burial and exhumation scenarios showed that muogenic production following basin excavation by the Yellow River at 0.5 Ma would, at maximum, increase observed burial ages by ~30%, but only if basin excavation was instantaneous and only for shallowly-buried (~15 m) samples (Craddock et al., 2010). For samples buried more deeply, and for slower rates of downcutting along the Yellow River, post-burial production due to muons will be less. In light of this sensitivity analysis, we estimate that our calculated burial ages are subject to ~15% uncertainty, which is within the analytical uncertainty on the calculations.

In order to compare the ^{26}Al/^{10}Be ratio and ^{10}Be concentration between sites, the abscissa in Figure 6 is normalized by the product of the ^{10}Be production rate at sea level and high latitude and the inverse of the local production rate (Granger, 2006). Solid curves represent ^{26}Al and ^{10}Be concentrations for various burial times (e.g. 1 Ma, 2 Ma, etc.). These contours are calculated assuming no post-burial production of muons, such that our calculated burial ages deviate slightly from these contours. It can be seen from the zero burial age curve that ^{26}Al and ^{10}Be are produced at a ratio of ~6.3, which is simply the ratio of P_{Al} to P_{Be}. Prior to transport, deposition, and burial, samples are eroded to earth's surface at some unknown rate. The sub-vertical, stippled lines represent the burial history for samples with various inherited erosion rates/cosmogenic inventories. The dashed curve represents ^{26}Al and ^{10}Be concentrations for samples experiencing constant exposure at earth's surface. Because unstable cosmogenic isotopes tend towards a secular equilibrium, there is a finite limit to the ^{10}Be concentration, which is located on the far right hand side of the burial time = 0 curves.

DATA REPOSITORY SECTION 4. PALEOMAGNETICS

Field methods

For both sections, 3-4 specimens were collected from each bed, using a gas-powered drill with a 2.5 cm diameter core bit. The core-plate orientation was measured using a magnetic compass. Bedding dip of sites was also measured using a magnetic compass. In certain stratigraphic intervals, the sediment was too friable to be sampled with a drill. At these sites, oriented block samples ~2 cm^3 in volume, were collected. These samples were carved into smaller cores in the laboratory.

Laboratory techniques

Magnetic and thermal cleaning was conducted at The California Institute of Technology. Magnetization was measured using a three-axis DCSQUID moment magnetometer in a magnetically shielded μ-metal room (Kirschvink et al., 2008). The background noise of the magnetometer is <1 pA m^2. It is equipped with a vacuum pick and put, computer-controlled sample changing system. After measuring the natural remnant magnetism of each specimen, most samples were subjected to up to 20 steps of alternating field (AF) and thermal (TT) demagnetization. Five or six evenly spaced AF steps, between 0 and 100 or 120 gauss were first applied in order to remove low coercivity viscous remnant magnetization (VRM). AF demagnetization was conducted with a computer-controlled, three-axis coil system. Following that, thermal steps at 70, 150, 250, 350, 450, 500, 530, 555, 570, 600, 635, 655, 670, and 680 °C were applied. Thermal demagnetization was conducted with a commercially built, magnetically shielded furnace. The treatment was designed to have a high density of steps leading up to the unblocking temperatures of magnetite and hematite (570 and 680 °C, respectively). For the lower section, 238 specimens were demagnetized, one from each of the 218 sites, and duplicate specimens from 20 sites. The duplicate measurements were made in order to obtain a higher density of thermal steps for sites with overlapping characteristic remnant magnetization (ChRM) and VRM (see below). For these samples, we implemented thermal steps at 70, 100, 120, 150, 190, 230, 260, 290, 320, 350, 425, 500, 530, 550, 560, 570, 615, and 665 °C. If the magnetization measurement following an AF or TT step yielded a circular standard deviation (CSD) of >15˚, the measurement was repeated up to two times. If a CSD of ≤15˚ could not be obtained, the data for the AF/TT step were discarded.

Low temperature/coercivity component and high temperature component directions were determined using a least-squares fit, principal component analysis (Kirschvink, 1980; Jones, 2002). In general, we sought to perform the least squares, principal component analysis on ≥ 4 TT/AF steps. Commonly, more steps were incorporated, however, in a few cases, only three TT/AF steps were used. For magnetization components that were believed to be characteristic, regression included the origin and were forced through the origin. We consider mean angular deviations for a regression that exceed 15 to indicate a poor quality regression, although this did not apply to any of our interpretable samples. Although some authors filter data with VGP latitudes of <30˚ (19 sites in the lower section), we choose not to do so simply because our magnetostratigraphy is unaffected by applying this filter. If brief polarity reversals occurred where segments overlapped, the stratigraphic height of specimens from a segment was adjusted in order to eliminate reversals. This correction was applied to six samples, four of which were corrected by <~2 m and two of which were corrected by ~6 – 7m. In order to apply this correction, the slight adjustment in height was forbidden if it altered the stratigraphic order of samples within a single stratigraphic segment. Because some stratigraphic intervals were only sparsely sampled, we did not reject single site reversals, although this filter is sometimes applied to other magnetostratigraphic data. After determining the orientation of the ChRM (the highest stability component of magnetization) for each sample, the declination and inclination were used to calculate the VGP position. Northern hemisphere poles were assigned normal polarity and southern hemisphere poles were assigned reversed polarity.

A small number of samples were subjected to a full battery of rock magnetic experiments. First, the NRM of samples was removed in alternating fields up to 1000 G. Subsequently, isothermal viscous remnant magnetizations (IRM) and anhysteric remnant magnetizations (ARM) were imparted and removed by IRM backfields and/or by AF cleaning.

Rock Magnetism

We divide our paleomagnetic specimens into three categories, which reflect the magnetic mineralogy of the specimens.

For many specimens (Type 1), hematite appears to be the dominant carrier of the highest stability (characteristic) component of the NRM (abbreviated ChRM hereafter) (Fig. A5). Although alternating fields of up to 1T are insufficient to remove the NRM of all of the specimens, these specimens preserved a relatively high percentage of their NRM during AF demagnetization (e.g. specimen 509.1, Fig. A5). Likewise, these samples do not reach saturation during isothermal remnant magnetism (IRM) acquisition up to 1000 G. In general, inability to clean the NRM in high alternating fields indicates the presence of antiferromagnetic minerals, such as hematite or goethite, thereby restricting the possible magnetic mineralogy of these specimens (see Lowrie, 1990 and references therein). For these specimens, the magnitude of the NRM was not appreciably diminished by AF steps up to 126 G followed by thermal steps up to 570 (e.g. specimen 509.1, Fig. A5). Magnetization was abruptly removed between TT steps 570 to 680 ºC. Given that goethite has an unblocking temperature of ~80 - 120° C and hematite has an unblocking temperature of ~675° C (Lowrie, 1990 and references therein), hematite is most likely to carry the ChRM. Commonly, these specimens display stable magnetization directions on Zjiderfeld and equal area plots to thermal steps between 570 and 680 ºC. Moreover, a low stability component of NRM is typically removed at low AF steps (below 126 G) or sometimes low temperature steps (70 - 150 ºC), suggesting that the overprint is carried by low coercivity magnetic minerals, such as magnetite, titanomagnetite, maghemite, and/or goethite. For a subset of Type 1 specimens, the magnetization appears to be carried primarily by magnetite, rather than hematite (specimen 918.1, Fig. A5). Compared to the specimens described above, AF demagnetization up to 126 G removes a relatively high proportion of the NRM, and the specimens tend to show that a high percentage of the NRM is removed between 500 and 570 ºC, immediately below the unblocking temperature of magnetite (580 ºC). Furthermore, the specimens often exhibit unstable behavior above thermal steps of 555-570 ºC. Similar to other type 1 specimens, alternating fields of 60-100 mT or temperatures of 70-150 ºC typically remove a viscous overprint from these samples, suggesting that low coercivity minerals, such as magnetite and/or goethite carry the viscous remnant magnetism (VRM).

The ChRM of a second type of specimens (Type 2) appears to be carried by titanomagnetite and/or maghemite (Fig. A5). These samples exhibit much lower coercivities during AF demagnetization in fields up to 1T and during IRM acquisition in fields up to 1T, suggesting a relatively low proportion of antiferromagnetic minerals (e.g. sample 702, Fig. A5). During thermal demagnetization, these specimens exhibit a pronounced drop in magnetization at ~200 – 350 ºC (Fig. 7), which is similar to the maximum unblocking temperature of titanomagnetite and maghemite (~350° C). Often, this type of specimen displays unstable demagnetization behavior at thermal steps at or above 200 - 350 ºC (e.g. sample 702, Fig. 7), suggesting that minerals with relatively high unblocking temperatures, such as magnetite and/or hematite, do not carry the ChRM. Importantly, this type of sample exhibits a pronounced drop in the NRM at low AF levels, indicating that the minerals that carry the ChRM also carry a viscous overprint. Therefore, the stability spectrum of the VRM partially or completely overlaps the ChRM. In light of this observation, the ChRM of type 2 specimens, which exhibit overlapping VRM and ChRM stability spectra, was determined using the magnetization circle method described by McFadden and McIlhenny (1988).

We did not attempt to interpret the polarity for a small subset of specimens (Type 3) for two reasons. 1) The stepwise demagnetization behavior for a few sites was too erratic to interpret for some sites. 2) The magnetic inclination and the magnetic declination suggested opposing polarities for some sites.

To more closely examine the demagnetization behavior of samples exhibiting with similar, or completely overlapping, stability spectra for the ChRM and the VRM, we conducted an additional set of thermal demagnetization experiments on duplicate specimens, with a high concentration of thermal steps between 70 and 350 degrees. Every one of these samples indicates 1) stable, interpretable magnetization directions below 200 - 350 ºC, 2) a sharp drop in magnetization around 350 ºC, and 3) unstable directions above 200 - 350ºC (see specimen 702.4, Fig. A5). The clear demagnetization behavior of these samples substantiates our inference that the ChRM of these specimens is carried by titanomagnetite and/or maghemite, and that the stability spectra of the ChRM and VRM should overlap for these samples. Moreover, all sites with duplicate specimens yielded consistent polarity directions, suggesting that our polarity determinations are robust.

Figure A6 shows the end-member NRM-removal and IRM-acquisition behaviors in alternating fields for samples subjected to the full battery of rock magnetic experiments. Samples that retain a relatively high proportion of NRM in an alternating field, and that develop a relatively small IRM during IRM acquisition are interpreted to have a high proportion of hematite.

Sample information

Tables A1 and A2 show latitude, longitude, elevation, stratigraphic height and characteristic remnant magnetization information for each sample.

REFERENCES

Braucher, R., Brown, E. T., Bourles, D. L., and Colin, F., 2003, In situ produced ^{10}Be measurements at great depths: implications for production rates by fast muons: Earth and

Planetary Science Letters, v. 211, no. 3-4, p. 251-258.

Craddock, W. H., Kirby, E., Harkins, N., Zhang, H., Shi, X., and Liu, J., 2010, Rapid fluvial incision along the Yellow River during headward basin integration: Nature Geoscience, v. 3, p. 209-213, doi: 10.1038/NGEO777.

Davis, M., Matmon, A., Fink, D., Ron, H., and Niedermann, S., 2011, Dating Pliocene lacustrine sediments in the central Jordan valley, Israel - Implications for cosmogenic burial dating: Earth and Planetary Science Letters, v. 305, p. 317-327, doi:10.1016/j.epsl.2011.03.003.

Granger, D. E., 2006, A review of burial dating methods using ^{10}Be and ^{26}Al., in Siame, L. L., Bourles, D. L., and Brown, E. T., eds., In situ-Produced Cosmogenic Nuclides and Quantification of Geological Processes: Boulder, CO, Geological Society of America, p. 1-16.

Granger, D. E., and Muzikar, P. F., 2001, Dating sediment burial with in situ-produced cosmogenic nuclides: theory, techniques, and limitations: Earth and Planetary Science Letters, v. 188, no. 1-2, p. 269-281, doi:10.1016/S0012-821X(01)00309-0.

Granger, D. E., and Smith, A. L., 2000, Dating buried sediments using radioactive decay and muonogenic production of ^{26}Al and ^{10}Be: Nuclear Instruments and Methods in Physics Research Section B: Beam Interactions with Materials and Atoms, v. 172, no. 1-4, p. 822-826.

Jones, C. H., 2002, User-driven integrated software live: "PaleoMag" paleomagnetics analysis on the Macintosh: Computers and Geosciences, v. 28, no. 10, p. 1145-1151.

Kirschvink, J. L., 1980, The least-squares line and plane and the analysis of palaeomagnetic data: Geophysical Journal of the Royal Astronomical Society, v. 62, no. 3, p. 699-718.

Kirschvink, J. L., Kopp, R. E., Raub, T. D., Baumgartner, C. T., and Holt, J. W., 2008, Rapid, precise, and high-sensitivity acquisition of paleomagnetic and rock-magnetic data: Development of a low-noise automatic sample changing system for superconducting rock magnetometers: Geochemistry, geophysics, geosystems, v. 9, no. Q05Y01, doi: 10.1029/2007GC001856.

Lowrie, W., 1990, Identification of ferromagnetic minerals in a rock by coercivity and unblocking temperature properties: Geophysical Research Letters, v. 17, no. 2, p. 159 – 162.

McFadden, P. W., and McElhinny, M. W., 1988, The combined analysis of remagnetization circles and direct observations in paleomagnetism: Earth and Planetary Science Letters, v. 87, no. 1-2, p. 161-172, doi: 10.1016/0012-821X(88)90072-6.

Nishiizumi, K., Imamura, M., and Caffee, M. W., 2007, Absolute calibration of ^{10}Be AMS standards: Nuclear Instruments and Methods in Physics Research Section B: Beam Interactions with Materials and Atoms, v. 258, no. 2, p. 403-413,

Norris, T. L., Gancarz, A. J., Rokop, D. J., and Thomas, K. W., 1983, Half-life of ^{26}Al: Proceedings of the Fourteenth Lunar and Planetary Science Conference, Part 1, Journal of Geophysical Research, v. 88, p. B331-B333.

Ochs, M., and Ivy-Ochs, S., 1997, The chemical behavior of Be, Al, Fe, Ca, and Mg during AMS target preparation from terrestrial silicates modeled with chemical speciation calculations: Nuclear Instruments and Methods in Physics Research Section B: Beam Interactions with Materials and Atoms, v. 123, no. 1-4, p. 235-240,

Stone, J. O., 2000, Air pressure and cosmogenic isotope production: Journal of Geophysical Research Solid Earth, v. 105, no. B10, p. 23,753-23,759.

Wolkowinsky, A. J., and Granger, D. E., 2004, Early Pleistocene incision of the San Juan River, Utah, dated with ^{26}Al and ^{10}Be: Geology, v. 32, no. 9, p. 749-752, 10.1130/G20541.1.

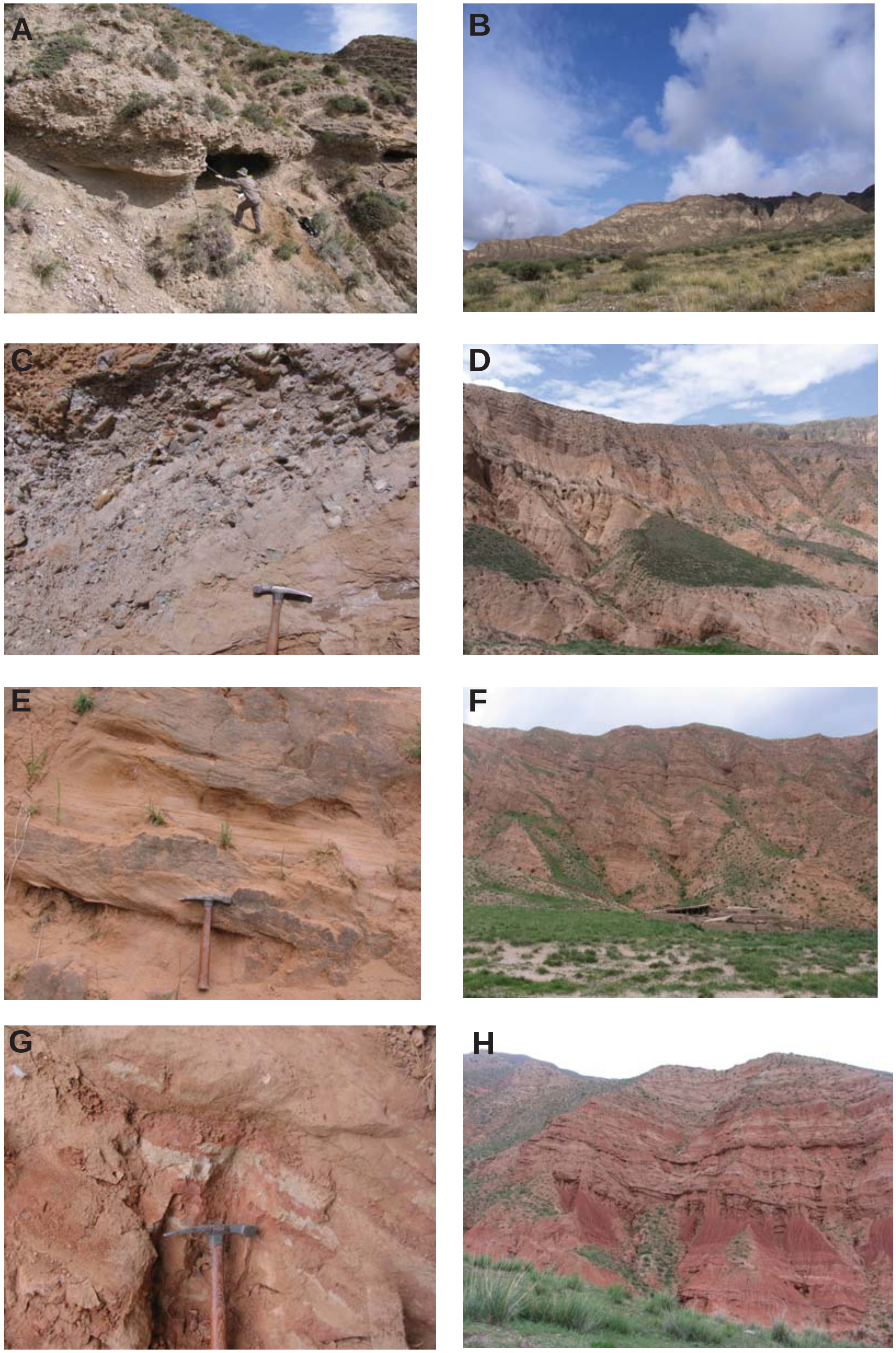

Figure A1. Stratigraphic units in lower levels of southern Gonghe subbasin. (A), (B) Lithostratigraphic unit 3. (C),(D) Lithostratigraphic unit 2. (E), (F) Lithostratigraphic unit 1a. (G), (H) Lithostratigraphic unit 1. Cliffs in (D), (F), and (H) are on the order of ~200 m high.

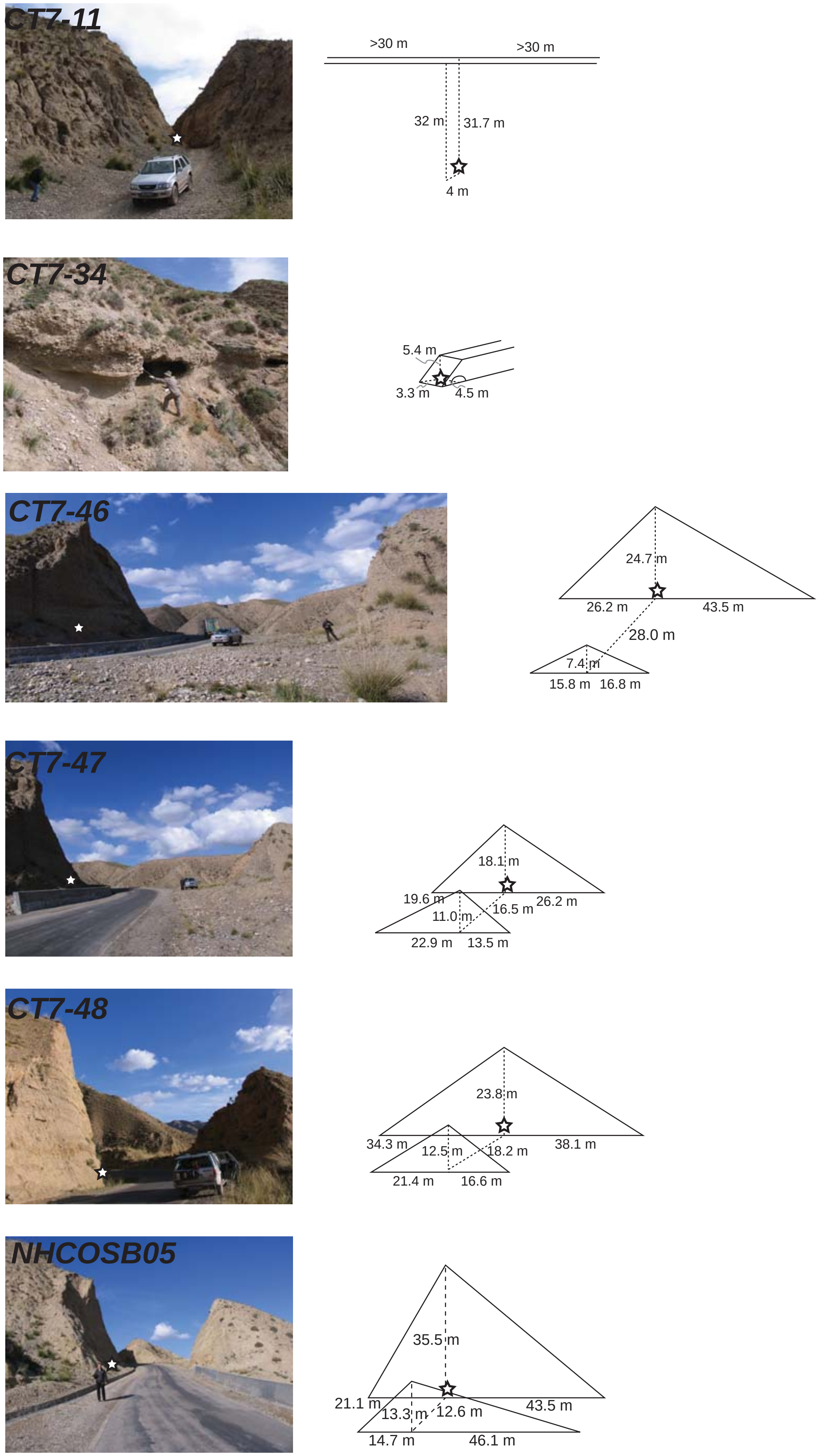

Figure A2. Cosmogenic burial age sample sites. Sample locations marked with open stars.

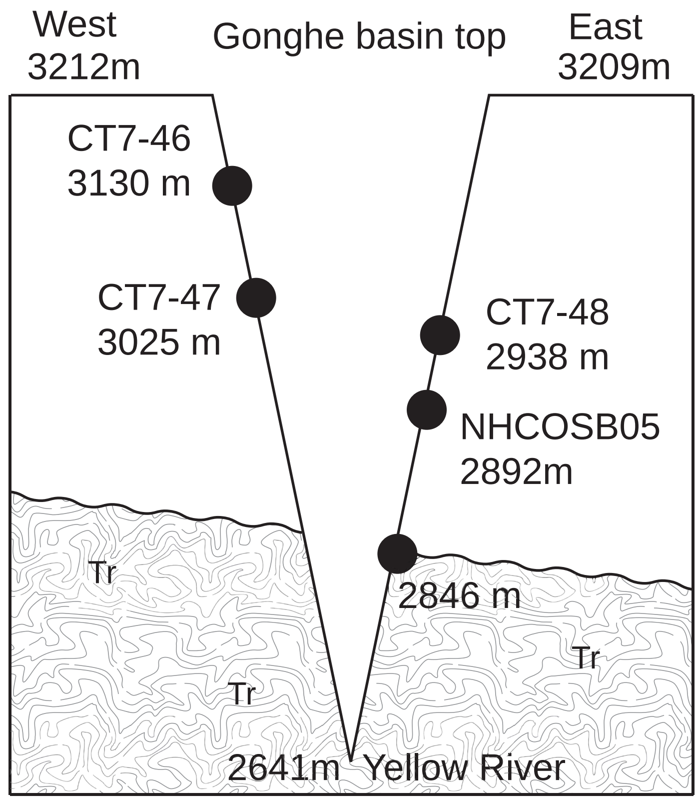

Figure A3. Schematic diagram showing depth of L3 burial age samples.

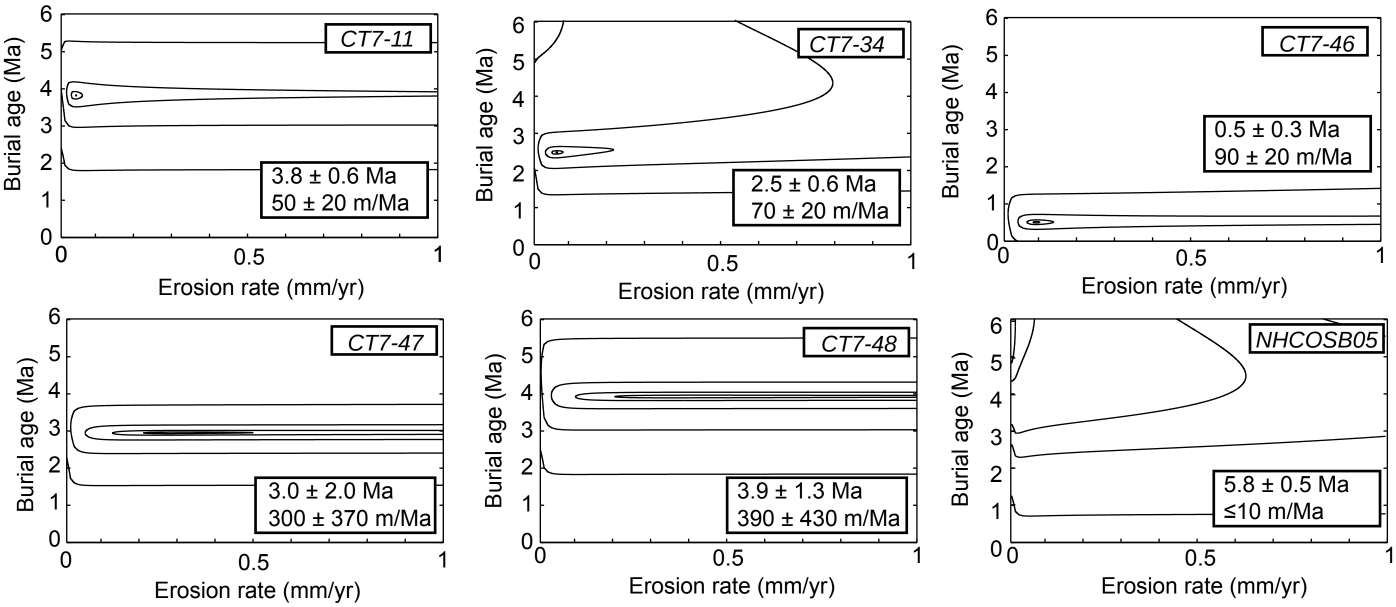

Figure A4. Contour plots of chi-squared statistics for combinations of burial age and erosion rate. Both burial age and erosion rate misfits are normalized such that an error of 1 is the largest error for a model iteration. Each contour represents a 1-order of magnitude decrease in the size of the chi squared statistic. In the NHCOSB05 plot, each contour represents a half-order of magnitude decrease in the chi squared statistic.

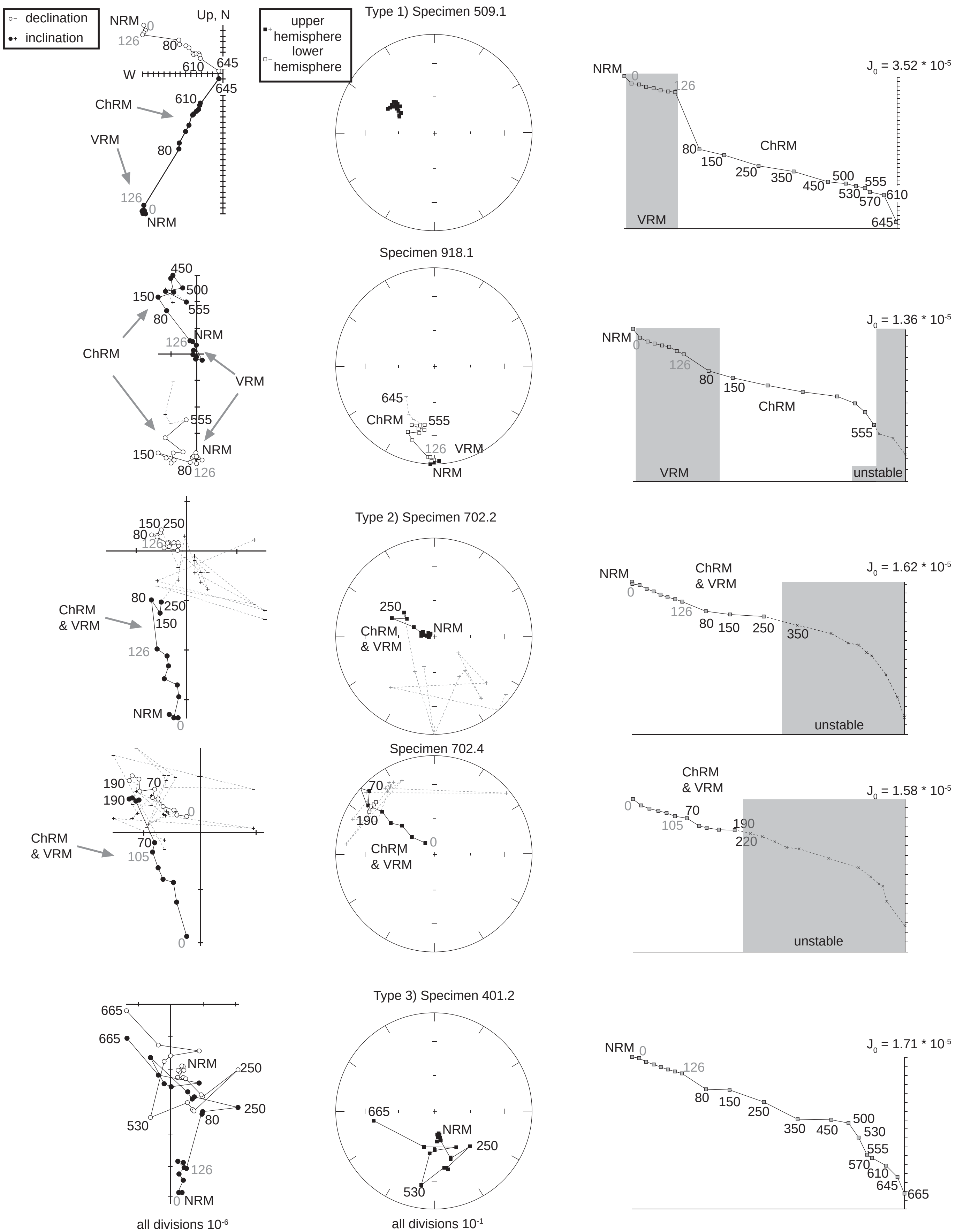

Figure A5. Example orthogonal vector, equal area, and magnetization intensity plots for representative samples from the southern Gonghe stratigraphic sections.

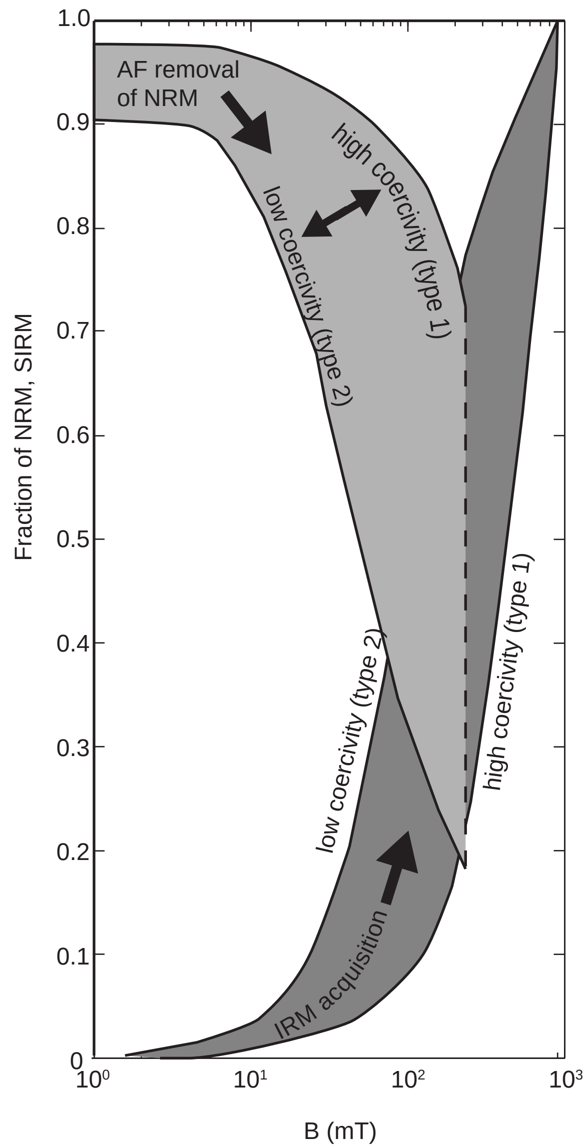

Figure A6. Alternating field removal of NRM and IRM acquisition curves. Y-axis represents the proportion of the total NRM, or the Saturation IRM, respectively.

TABLE A1. SUPPLEMENTARY PALEOMAGNETIC INFORMATION-LOWER SECTION

Sample	Latitude (°)	Longitude (°)	Elevation (m)	Type	Dec. (g)	Inc. (g)	Dec. (t)	Inc. (t)	N	MAD	Stratigraphic Height (m)	Declination	VGP Latitude (°)
101.2	35.70599	100.16951	3062	ChR	286.9	62.1	359.7	58.1	7	1.9	169.3	-0.3	86
102.2	35.70596	100.16959	3056	Cir	85.8	-69.1	36.8	-88	12	90	173.2	36.8	-32
103.1	35.7059	100.16946	3105	ChR	291.3	41.4	329.9	47.2	5	4.9	176.1	-30.1	64
104.3	35.70568	100.1693	3096	ChR	279.7	51.6	338.3	59.1	5	2.8	179.7	-21.7	72
105.3	35.70617	100.16956	3068	ChR	344.6	37.1	0.6	15.2	4	6	182.6	0.6	63
106.1	35.70617	100.16956	3071	ChR	310.8	59.2	1.6	46.2	9	2.5	187.6	1.6	82
107.2	35.7063	100.16938	3083	ChR	265	46.7	321.6	67.2	9	4.1	192.9	-38.4	58
108.3	35.70635	100.16956	3083	ChR	255.6	60.9	10.8	74.5	10	2.1	199.6	10.8	63
109.3	35.70634	100.16957	3083	ChR	290.4	59.8	2.4	59	4	3.4	204.1	2.4	85
110.1	35.70631	100.16955	3125	ChR	258.7	61.1	13.3	75.1	4	9.2	209	13.3	62
112.3	35.70646	100.16923	3080	Cir	121.9	-47.1	165.7	-47.8	11	12.3	215.4	165.7	-76
113.3	35.70654	100.16933	3084	Cir	94.8	-50.1	143.8	-61.2	10	22.2	219.5	143.8	-61
114.1	35.70656	100.16921	3112	ChR	275.7	55.5	353	71.6	6	2.6	223.3	-7	68
115.3	35.7066	100.1692	3100	ChR	316.1	31.9	341.5	36.5	6	6.4	231.9	-18.5	68
118.3	35.70652	100.16921	3143	Cir	125	-67.9	212.4	-61.3	13	6.2	248.7	212.4	-64
120.1	35.70669	100.16948	3129	ChR	199.5	-51.7	219.2	-23.8	4	10.4	263.1	219.2	-48
121.1	35.70675	100.16958	3133	Cir	68.3	-49.3	97.8	-67.6	12	37.8	269.8	97.8	-31
122.1	35.70675	100.16958	3133	Cir	73.9	-53.9	178	-88.5	12	9.4	271.3	178	-38
123.2	35.70674	100.16956	3134	ChR	251.9	56.7	56.6	87.1	4	1.8	273.3	56.6	38
124.1	35.70678	100.16958	3140	ChR	338.3	59.5	23.4	44.8	7	12.8	277.4	23.4	68
126.3	35.70674	100.16976	3179	Cir	80.5	-78.9	234	-72.2	12	20	290.1	234	-48
127.3	35.70662	100.16972	3207	ChR	92.2	-56.3	169.7	-74.7	4	4.4	293.4	169.7	-63
200.3	35.70633	100.17165	3246	ChR	137.2	-36.3	165	-37.7	4	2	295.4	165	-71
201.3	35.70676	100.1723	3284	Cir	91.6	-75	209	-72.1	4	7.1	297	209	-61
204.1	35.70694	100.17168	3075	ChR	292.3	54.4	345.4	60.6	7	5.4	305.3	-14.6	77
205.1	35.70691	100.17161	3118	Cir	137.5	-46.2	170.3	-40	11	7.5	308.6	170.3	-75
206.2	35.70663	100.17147	3160	ChR	266.5	39.1	292.7	63	7	3.3	311.6	-67.3	39
207.2	35.70644	100.1715	3203	ChR	307.5	32.4	329.2	38	8	15	315.7	-30.8	60
208.2	35.7071	100.17167	3086	ChR	21.6	41	30.5	15.2	5	14.5	317.5	30.5	51
209.2	35.70713	100.17167	3083	ChR	42.1	65.9	50.9	37.1	5	11.4	319.7	50.9	43
210.1	35.70718	100.17167	3083	ChR	276.5	75.4	30.6	71.6	6	7.9	322.8	30.6	60
211.2	35.70713	100.17167	3125	Cir	126.4	-40.7	154.4	-38.7	13	8.3	328.7	154.4	-64

212.1	35.70714	100.17166	3125	Cir	160.1	-62.8	196.3	-42.8	15	20.6	332.2	196.3	-73
213.2	35.70718	100.17186	3166	Cir	102.1	-57.5	151.8	-69.3	14	11	335.6	151.8	-63
214.1	35.70718	100.17184	3166	Cir	73.5	-56	104	-80	16	11.9	337.7	104	-37
215.3	35.70719	100.17183	3116	Cir	139.5	-55.4	176	-52.1	12	8	340	176	-86
216.4	35.7073	100.17175	3106	ChR	295.2	50.4	331.4	58.9	13	3.7	342	-28.6	67
217.1	35.70736	100.17171	3103	ChR	208.8	-47.6	217.8	-24.4	4	7.6	346.7	217.8	-49
218.2	35.70736	100.17177	3109	Cir	146.3	-30.9	166	-27	10	7.6	349.6	166	-66
219.3	35.70736	100.17182	3103	Cir	187.8	-82.3	228.7	-52.6	11	8.7	353.1	228.7	-50
220.1	35.7073	100.17186	3127	Cir	143.6	-50	177.5	-40.8	9	13.8	356.4	177.5	-78
221.3	35.70735	100.17172	3137	Cir	120.8	-58	161.2	-57.6	12	19.4	359.2	161.2	-75
222.1	35.70737	100.17174	3132	Cir	124	-44.4	155.1	-43	11	15	362.9	155.1	-66
223.3	35.70749	100.17183	3115	Cir	190	-75.2	218.5	-46.3	11	10	365.8	218.5	-57
224.2	35.70732	100.17184	3155	Cir	68.2	-9.4	73.9	-40.6	4	23.2	381.4	73.9	-1
225.1	35.7076	100.17169	3183	Cir	197.1	-75.7	218.1	-46.6	14	8.8	386	218.1	-57
226.4	35.70766	100.17172	3183	Ch2	35.6	74.6	39.3	36.5	5	4.3	388.4	39.3	53
228.1	35.70818	100.1719	3219	ChR	26.1	76.2	36.6	38.4	4	5.2	395.6	36.6	55
228.3	35.70774	100.17165	3142	ChR	219.7	47.9	207.5	85.9	3	1.2	395.6	207.5	28
229.4	35.70776	100.17148	3171	ChR	96.1	74.7	55.2	40.7	4	3.5	398.5	55.2	41
230.2	35.70737	100.17157	3191	ChR	121.6	-61.2	174.3	-42.5	5	5.1	401	174.3	-79
232.3	35.70768	100.17152	3182	ChR	314.2	13	319.4	0.6	4	7.3	406.4	-40.6	39
233.1	35.70782	100.17159	3170	ChR	224.8	59	0.3	74.9	4	3.5	410.1	0.3	63
233.2	35.70782	100.17159	3170	ChR	94.1	44	72.6	16.7	6	6.9	410.1	72.6	19
234.1	35.70786	100.17159	3171	Cir	153.7	-44.8	169.1	-14.5	5	2.2	414.2	169.1	-61
234.3	35.70786	100.17159	3171	Cir	278.3	-72.5	230.2	-54.7	11	12.6	414.2	230.2	-49
235.1	35.7079	100.17162	3166	Cir	108.9	-27.6	128.7	-47.6	10	8.5	416.9	128.7	-46
236.3	35.70793	100.17182	3164	ChR	328	63.3	1.8	31.5	4	4.9	422.2	1.8	72
237.3	35.70805	100.17183	3162	ChR	9.9	83.1	26.6	42.7	4	6.6	426.6	26.6	65
301.2	35.70813	100.17735	3024	ChR	266.2	67.7	353.8	64	5	8	428.4	-6.2	78
302.2	35.70826	100.17724	3000	ChR	250.9	62.8	345.2	70.5	4	7.2	431.3	-14.8	68
238.3	35.70801	100.17187	3162	ChR	293.8	42.3	326.7	34.9	4	8.8	434.2	-33.3	57
239.2	37.70808	100.17186	3165	ChR	302.8	65.8	355.6	44.9	5	5.9	436	-4.4	81
303.1	35.70832	100.17708	2995	ChR	341.8	28.2	350.6	4.4	3	6.5	436.5	-9.4	56
303.4	35.70832	100.17708	2995	ChR	51.7	62.8	44.7	26.1	5	6.2	436.5	44.7	45
240.1	35.70776	100.17172	3190	ChR	24.2	82.5	30.1	45.2	4	5.6	439.1	30.1	63

304.4	35.70831	100.1771	3009	ChR	279.2	22.5	297	33.9	7	7.5	439.1	-63	32
305.1	35.7083	100.17691	3029	ChR	75.8	73	51.9	41.6	6	9.2	442.2	51.9	44
241.3	35.70804	100.17197	3173	ChR	105.8	70.4	58.9	44.8	4	5.9	445.7	58.9	39
306.2	35.70822	100.17702	3016	ChR	309.3	74	10.5	53.5	4	3.3	445.8	10.5	81
307.4	35.70838	100.17713	3006	ChR	291.5	71.6	5.2	57.1	4	3.8	447.2	5.2	85
242.4	35.70808	100.17198	3173	ChR	112.7	-40.8	142.6	-37.4	3	10	448.6	142.6	-54
243.3	35.70807	100.17197	3181	Cir	128.8	-41.3	150.3	-38.5	10	5.6	451.1	150.3	-61
244.2	35.70807	100.1721	3179	ChR	131.8	-32.5	148.9	-22.5	7	10.7	454	148.9	-53
309.2	35.70359	100.17695	3027	ChR	264.9	61.6	344.4	66.1	4	7.3	454.3	-15.6	72
310.1	35.70863	100.17699	3030	ChR	299.4	75.5	15.5	55.3	6	10.9	458.7	15.5	77
311.1	35.70868	100.17662	3027	ChR	269.1	46.8	317.8	59.8	8	9.4	459.8	-42.2	57
245.1	35.70815	100.17206	3183	ChR	310.4	64.3	355.1	47.2	6	4.1	464.5	-4.9	82
314.2	35.70883	100.17649	3033	ChR	346.9	65.9	15.1	39.2	4	13.7	466.2	15.1	72
315.2	35.70887	100.17646	3036	ChR	279.3	44.2	315.5	51.8	5	5.9	471	-44.5	53
316.2	35.70891	100.1764	3042	ChR	284.6	69.5	358.5	60.6	4	9.8	476.2	-1.5	83
317.3	35.70893	100.17638	3043	ChR	317.9	50.8	346.9	36.9	4	4.4	478.4	-13.1	72
402.3	35.70826	100.17846	3006	ChR	342.7	43.6	354.9	23.3	6	5.3	480.7	-5.1	67
403.1	35.70833	100.17845	3004	Cir	110.2	-72	185.2	-59	10	4.7	485.8	185.2	-84
404.1	35.70834	100.17848	3008	Cir	137.8	-46.3	157.7	-34.9	12	11.7	489.3	157.7	-65
319.4	35.7091	100.17634	3046	Cir	65.2	-64.7	178.9	-76.8	12	10.9	489.6	178.9	-60
320.4	35.70899	100.17615	3072	Cir	146.7	-50.1	170.1	-32.6	10	9.5	491	170.1	-71
321.2	35.70898	100.17609	3081	ChR	110.6	-3.7	113.7	-9.1	7	11.7	492	113.7	-22
405.3	35.70845	100.17865	3012	ChR	270.8	51	313.1	56.7	4	2.7	493.4	-46.9	52
406.2	35.7084	100.17849	3014	ChR	4.4	61.3	17.7	32.4	5	9.8	496	17.7	67
407.3	35.70851	100.17833	3015	ChR	274.7	53.9	324.1	57.4	5	5.3	499.2	-35.9	61
408.1	35.70843	100.17845	3015	ChR	24.2	31	26.1	-1.3	5	4.4	501.4	26.1	47
409.3	35.70851	100.17843	3047	ChR	299.1	52.6	339.9	45.8	6	10.5	507.1	-20.1	71
410.3	35.70855	100.17846	3033	Cir	154.2	-68.9	191	-47.2	10	2.2	511.3	191	-79
412.2	35.70867	100.17845	3019	ChR	278.5	51.4	330.6	58	8	12.9	518.9	-29.4	66
413.4	35.70881	100.17821	3032	ChR	282.2	55.2	339.4	58.2	5	5.7	526.3	-20.6	73
414.1	35.70881	100.17824	3035	ChR	291.4	55.9	345.8	54.9	4	3.6	530	-14.2	78
415.2	35.70894	100.17824	3042	Cir	3.3	-63.7	284.9	-72	11	12.3	533.1	-75.1	-21
415.3	35.70894	100.17824	3042	Cir	92.2	-61.5	167.3	-65.5	10	9.4	533.1	167.3	-74
416.3	35.70895	100.17819	3036	Cir	352.2	-45.2	328.2	-60	10	10.1	537	-31.8	9

416.2	35.70895	100.17819	3036	ChR	272.2	13.6	284.7	35.4	3	9.5	537	-75.3	23
417.2	35.7089	100.17815	3033	ChR	93.2	82.4	55.6	50.4	5	9.9	539.9	55.6	44
418.1	35.70893	100.17823	3036	ChR	334.3	48.9	359.4	30.6	6	3.7	542.4	-0.6	71
500.1	35.709	100.17889	3030	ChR	237.5	74.7	31.6	70.5	4	6.2	544.4	31.6	61
501.3	35.70902	100.17885	3026	Cir	133	-72.5	190	-53.3	10	6.9	546.6	190	-82
419.2	35.70899	100.17823	3046	Cir	136	-44.9	163.3	-38.8	10	10	546.7	163.3	-70
502.4	35.709	100.17832	3022	Cir	175.4	-84.2	212.5	-55.4	10	7.5	549.3	212.5	-64
502.2	35.709	100.17832	3022	ChR	230.4	-68.3	225.2	-35.5	7	11.9	549.3	225.2	-47
503	35.70906	100.17882	3026	Cir	98	-46.2	139.1	-58.2	6	8.3	552.9	139.1	-57
504.1	35.70807	100.1788	3030	ChR	344.5	32.1	354.7	12.6	6	32	555.7	-5.3	61
504.4	35.70807	100.1788	3030	ChR	244.7	51.1	290.8	74.4	5	1.4	555.7	-69.2	40
505.3	35.709	100.17879	3034	ChR	266.2	45.5	303	59.9	4	7.8	558.1	-57	45
506.4	35.70911	100.17877	3042	Cir	150.1	-57.2	178.6	-41.3	9	9.9	560.1	178.6	-79
507.3	35.70921	100.17874	3044	ChR	185.2	73.2	79	73.3	8	2.8	562.9	79	35
507.4	35.70921	100.17874	3044	ChR	270.3	24.1	284.4	39.8	6	12.5	562.9	-75.6	24
508.4	35.70913	100.17871	3054	ChR	304.9	63.5	350.2	56.3	8	5.5	565.9	-9.8	82
509.1	35.70918	100.17867	3055	ChR	281.7	42.1	305.9	51.1	9	2.3	570.7	-54.1	45
600.2	35.70852	100.18083	3056	ChR	303.9	46.6	328.3	48.5	9	3.6	571	-31.7	63
700.4	35.70847	100.18449	2946	ChR	187.8	-49	205.2	-29.7	11	3.4	571.1	205.2	-60
701.4	35.70858	100.18441	2954	Cir	127.6	-51.1	166.5	-53.5	11	8.8	575.1	166.5	-79
701.2	35.70858	100.18441	2954	Cir	27.7	-68.5	300.8	-75.2	11	14.1	575.1	-59.2	-18
601.3	35.70866	100.18086	3048	Cir	157.8	-66	195.4	-46.7	10	11.5	575.6	195.4	-75
702.2	35.70875	100.18439	2953	Cir	70.1	-56.8	102.7	-86.2	12	11.6	577.9	102.7	-36
702.4	35.70875	100.18439	2953	Cir	84.3	-54	133	-78.5	11	5.8	577.9	133	-48
511.4	35.70925	100.17861	3067	ChR	72.8	71.9	59.3	50.9	9	6.8	578	59.3	41
512.1	35.70926	100.1785	3069	ChR	49.6	56.9	49.4	35.9	8	8.9	579.1	49.4	44
703.1	35.70889	100.18434	2954	ChR	329.3	40.4	354.6	38.3	3	3.4	580.9	-5.4	76
703.3	35.70889	100.18434	2954	ChR	322.3	55.3	4.8	52.1	4	6.5	580.9	4.8	85
602.3	35.70864	100.18067	3048	ChR	310.5	84.6	39.3	68.6	10	8.5	581.4	39.3	57
704.3	35.70896	100.18431	2955	ChR	210.2	-40	218.8	-15.6	3	6.2	587.3	218.8	-45
800.1	35.70832	100.18418	2979	ChR	356.3	27.1	6.8	15.2	4	10.7	588.3	6.8	62
800.2	35.70832	100.18418	2979	ChR	51.3	79.5	63.3	50.8	5	10.9	588.3	63.3	38
705.1	35.70914	100.18427	2954	ChR	359.1	32.7	11.9	19	3	10.9	590.2	11.9	63
605.2	35.70898	100.18083	3023	Cir	198.9	-70.3	218.9	-48.4	13	11.4	590.7	218.9	-57

801.1	35.70836	100.18574	2949	Cir	114.5	-58.1	171.7	-66.8	9	6	590.8	171.7	-74
801.4	35.70836	100.18574	2949	ChR	138	-19.8	150.5	-26.9	5	3.8	590.8	150.5	-56
606.2	35.70903	100.18083	3023	Cir	117.9	-35.8	142.5	-37.3	11	5.7	593.7	142.5	-54
706.4	35.70925	100.1842	2953	ChR	262.9	42.6	280.7	69.6	3	7.1	594.3	-79.3	33
802.3	35.70844	100.18574	2952	ChR	301.7	85.1	59.2	63.6	5	13	594.7	59.2	45
607.2	35.70909	100.18083	3023	ChR	329.1	68.8	18.8	57.5	5	3.7	596.3	18.8	75
803.3	35.70844	100.18578	2948	ChR	220.9	70	107.6	75.8	5	3.8	599.7	107.6	24
707.3	35.70935	100.1842	2979	ChR	269.7	41.1	291.4	66.1	4	5.3	600.5	-68.6	39
804.2	35.70859	100.1858	2965	ChR	346	65.4	28	50.1	3	4.9	601.6	28	66
804.3	35.70859	100.1858	2965	ChR	198.9	78.2	91.5	66.9	4	5.1	601.6	91.5	25
805.1	35.70858	100.18586	2964	ChR	300.9	47.6	338.2	57.5	5	13.3	604.9	-21.8	72
708.4	35.70934	100.18418	2979	ChR	246.9	-39.4	247.1	-10.4	4	5.6	605	247.1	-22
806.2	35.7086	100.18585	2965	ChR	86.1	-61.7	170.6	-81.3	4	5.4	608.8	170.6	-52
808.4	35.70855	100.18591	2977	Cir	147.6	-61.7	195.4	-51	12	10.4	614.6	195.4	-77
809.1	35.70856	100.18591	2985	Cir	119.3	-58.2	159.2	-59	8	8.4	617.3	159.2	-73
810.2	35.70855	100.18595	2983	ChR	253.8	-38.2	251.2	-12.7	3	7.3	621.8	251.2	-19
811.2	35.70866	100.18598	2982	Cir	90.4	-34.2	108.6	-51.4	11	35.7	626.3	108.6	-32
813.4	35.70869	100.18599	2987	Cir	71.6	-41.4	89.4	-60.3	10	10.6	632.5	89.4	-22
814.1	35.7087	100.18599	2994	Cir	94.6	-48.9	126.4	-60.1	4	15.5	635.5	126.4	-48
815.2	35.70875	100.18604	2990	CiR	121.4	-39.7	142.5	-42.3	2	0	641.5	142.5	-56
816.2	35.70876	100.18607	2993	Cir	92.5	-29.3	107	-41.8	11	9.4	645.1	107	-27
817.2	35.70881	100.18618	3002	ChR	152	-35.9	164.1	-24.9	4	12.2	649.3	164.1	-64
818.3	35.7089	100.18669	2979	Cir	102.4	-56.6	138.2	-59.4	10	17.7	653.5	138.2	-57
819.1	35.70898	100.18663	2983	ChR	318.2	25	326.1	18	10	3.3	656.4	-33.9	50
820.1	35.70898	100.18665	2988	ChR	284.3	62.2	322.3	60.9	4	11.9	659.6	-37.7	60
821.2	35.70902	100.18661	3001	ChR	296.2	53.6	321.5	49.7	7	1.3	662.4	-38.5	58
822.1	35.70905	100.18659	2995	ChR	316.2	52.8	335.8	42.9	5	4.7	664.3	-24.2	67
823.2	35.70903	100.1865	2990	ChR	100	-30.5	112.6	-33.6	6	5.6	666.9	112.6	-29
824.1	35.7091	100.18651	2997	ChR	115.3	-31.7	127	-28.8	6	14.6	668.8	127	-39
826.3	35.70904	100.18638	3005	Cir	136.7	-44.9	154.4	-30.6	10	28.3	675.8	154.4	-61
827.3	35.7092	100.18619	3002	ChR	97.7	-28.1	110.4	-32	4	9.7	679.3	110.4	-26
828.1	35.70924	100.18612	3003	Cir	99.8	-23.2	108	-31.7	8	2.8	681.6	108	-24
828.8	35.70924	100.18612	3003	Cir	217.8	-51.3	215.9	-31	13	5.8	681.6	215.9	-53
829.2	35.70982	100.18651	2983	Cir	163.8	-78.6	198.8	-52.2	9	9.4	685.4	198.8	-74

901.2	35.7103	100.18879	2917	ChR	263.7	60.2	323.4	67.8	8	7	685.5	-36.6	59
830.1	35.70988	100.18643	2988	ChR	314.9	26	324.5	17.4	7	6.2	686	-35.5	48
830.4	35.70988	100.18643	2988	ChR	336.8	37.4	347.2	20.4	4	6.1	686	-12.8	63
831.3	35.70986	100.18643	2993	ChR	356.7	68.2	14.5	44.6	6	5.9	686.8	14.5	75
902.4	35.71033	100..18877	2921	Cir	179.2	-69.3	200.7	-44.4	8	8.6	687.8	200.7	-70
904.2	35.71038	100.18889	2923	ChR	108.7	-60.9	165.1	-58.4	4	8.4	695.8	165.1	-77
905.4	35.71028	100.18893	2914	Cir	155.3	-59.5	186.3	-41.8	7	10.5	698.7	186.3	-78
906.2	35.71044	100.18886	2929	ChR	311	27.6	327.2	24.6	12	5	701.8	-32.8	53
908.1	35.7105	100.18882	2929	ChR	14.9	31.4	19.4	2.6	5	7.8	707.8	19.4	52
909.2	35.71054	100.18873	2934	ChR	352.4	53.9	12	29.4	3	11.1	710.1	12	68
912.4	35.71072	100.18944	2912	ChR	277.9	39.7	309.8	51.5	4	6.8	710.3	-50.2	49
910.1	35.71057	100.18873	2932	ChR	245.9	83.7	38.7	63.7	6	2.5	713.1	38.7	59
913.2	35.71076	100.18939	2919	ChR	0.7	41.9	11.9	16.2	6	4.4	714.3	11.9	61
911.3	35.7106	100.1886	2932	ChR	279.7	24.5	298	38.5	4	7.2	717.1	-62	35
914.2	35.71079	100.1894	2926	Cir	94.2	-52.6	146.9	-63.1	5	6.8	717.1	146.9	-63
915.2	35.71087	100.18943	2926	ChR	291.1	50.3	332.6	51.7	7	9.8	720.9	-27.4	67
916.3	35.71088	100.18935	2926	ChR	60.6	53.2	54.6	22	4	6.1	728.2	54.6	35
917.4	35.71099	100.18934	2926	ChR	274.1	23.3	291.6	40.4	5	4.8	732.7	-68.4	30
918.1	35.71116	100.18919	2923	ChR	172	-58.7	194.5	-33.7	7	5	737.3	194.5	-69
919.1	35.71132	100.18907	2923	ChR	187.8	-60.6	204	-31.9	4	6.1	741.5	204	-62
920.2	35.71128	100.18908	2909	Cir	17.4	-78.9	237.1	-67.4	12	5.2	745.3	237.1	-47
921.3	35.71127	100.18904	2945	ChR	305.2	34.3	327.2	33	4	9.3	752.8	-32.8	56
922.3	35.71127	100.18904	2946	ChR	336.9	40.1	354.4	23.2	6	5	753.8	-5.6	67
922.4	35.71127	100.18904	2946	ChR	353.9	39.1	6.1	16	3	10.4	753.8	6.1	63
923.3	35.71129	100.18916	2982	Cir	129	-57.5	172.2	-49.3	6	5.6	755.3	172.2	-82
924.4	35.71126	100.18924	2976	ChR	6.6	40.5	15.8	14.4	5	4.9	761.5	15.8	59
925.1	35.71128	100.18923	2975	ChR	311.7	54.3	348.7	45.5	11	3.5	767.7	-11.3	77
1002.2	35.71108	100.19051	2928	Cir	141	-54.6	175.4	-43	11	12.1	772.7	175.4	-79
925.52	35.71139	100.18931	2968	ChR	77.5	42.9	69.4	15.2	4	9.1	775.7	69.4	21
926.2	35.71143	100.18932	2965	ChR	270.6	53.7	323.4	65.2	9	7	778.4	-36.6	60
1003.2	35.71113	100.1905	2932	ChR	358.6	56.6	17.3	32.4	8	2.7	778.6	17.3	67
1006.3	35.71137	100.19048	2952	ChR	103.2	68.8	72.1	45	4	6.8	801.9	72.1	29
1008.1	35.71135	100.19041	2983	ChR	1.2	39	11.6	15.9	4	6	813.1	11.6	61
1010	35.71166	100.19052	3000	ChR	34.6	42.4	33.5	12.5	5	3.3	822.1	33.5	48

1011	35.71162	100.19055	2995	ChR	65.9	55.9	52.1	29.3	7	8.3	825.6	52.1	40
1012	35.71161	100.19055	2982	ChR	43.2	36.1	43.9	6.2	6	3.4	831.4	43.9	38
1013.1	35.71168	100.19056	2986	ChR	273.9	57.7	332.1	66.3	5	8.7	839.6	-27.9	65
1013.3	35.71168	100.19056	2986	ChR	293.8	1.5	297.3	12.7	5	4.2	839.6	-62.7	26
1014	35.71168	100.19057	2955	ChR	263	48.1	302.6	57.8	5	13.2	841.1	-57.4	45

TABLE A2. SUPPLEMENTAL PALEOMAGNETIC INFORMATION-UPPER SECTION

Sample	Latitude (°)	Longitude (°)	Elevation (m)	Type	Dec. (g)	Inc. (g)	Dec. (t)	Inc. (t)	N	MAD	Stratigraphic Height (m)	Dec.	VGP Lat. (°)
1.3	35.69863	100.23183	2845	ChR	17.0	22.8	17.3	9.9	3	19.6	0.7	017	56
2.3	35.69868	100.23187	2842	ChR	186.3	-4.9	186.2	7.7	3	10.1	3.8	186	-51
3.2	35.69921	100.23197	2854	ChR	128.9	-67.2	152.5	-60.7	3	6.3	22.6	153	-68
4.1	35.69911	100.23186	2855	ChR	0.2	32.2	2.4	19.9	4	7.3	35.3	002	65
6.1	35.69974	100.23226	2890	ChR	75.4	32.2	70.7	25.3	6	20.4	54.6	071	23
5.1	35.69964	100.23212	2901	ChR	16.0	52.2	17.0	41.2	4	15.0	59.5	017	71
7.3	35.70039	100.23247	2874	ChR	346.4	41.4	350.5	33.0	14	3.6	70.1	-010	71
8.1	35.70017	100.23277	2905	ChR	342.8	20.5	344.5	12.5	9	11.1	75.2	-016	58
10.3	35.70144	100.23299	2968	ChR	353.5	13.5	354.2	6.4	4	9.4	99.5	-006	58
12.3	35.70175	100.233561	-	ChR	108.6	-17.2	110.3	-15.3	6	8.3	110.0	110	-21
11.1	35.70163	100.23310	2910	ChR	1.2	40.6	1.2	33.6	4	1.8	116.4	001	73
14.1	35.70225	100.23391	2981	ChR	92.8	-54.6	101.2	-54.1	5	5.7	131.8	101	-27
18.1	35.70255	100.23594	2900	Cir	162.3	-43.0	163.7	-38.3	7	6.8	141.5	164	-70
19.3	35.70290	100.23613	2900	Cir	165.6	-27.8	166.9	-23.3	8	4.5	145.1	167	-64
20.3	35.70295	100.23629	2938	ChR	59.8	52.2	54.7	49.3	4	12.0	148.0	055	44
21.2	35.70310	100.23614	2917	ChR	11.6	23.2	11.3	18.3	6	4.9	156.1	011	62
22.1	35.70312	100.23670	2926	ChR	311.7	80.3	325.5	77.4	4	14.7	166.4	-035	53
23.2	35.70334	100.23684	2931	Cir	145.0	-38.2	148.2	-34.1	6	14.3	175.9	148	-57
24.2	35.70338	100.23697	2937	ChR	300.7	60.5	306.4	58.3	4	1.2	179.8	-054	48
25.2	35.70326	100.23684	2930	Cir	146.0	-45.6	147.9	-41.8	3	8.5	183.8	148	-60
26.1	35.70380	100.23672	2948	Cir	154.7	-60.8	160.1	-57.6	5	9.6	195.4	160	-74
27.2	35.70380	100.23645	2988	Cir	201.7	-28.2	199.8	-23.6	4	6.5	226.5	200	-61
30.1	35.70500	100.239088	-	ChR	350.8	65.6	351.5	63.6	4	9.0	258.4	-009	78
31.1	35.70497	100.238935	-	ChR	347.2	41.5	347.6	39.5	4	3.3	261.9	-012	73
32.1	35.70501	100.239348	-	ChR	189.7	-48.5	189.4	-46.5	3	9.6	263.4	189	-79
33.2	35.70506	100.239306	-	ChR	166.3	-38.0	166.8	-36.1	13.2	-118.0	269.0	167	-71
34.3	35.70576	100.23903	2992	ChR	181.0	-47.1	181.6	-45.7	10	6.6	294.0	182	-82
35.2	35.70669	100.23927	3030	Cir	159.4	-50.3	163.8	-46.3	11	9.3	303.8	164	-74
36.2	35.70652	100.25972	3051	ChR	146.0	-30.0	146.7	-29.1	6	8.8	305.3	147	-54
38	35.70745	100.23893	3033	ChR	353.7	44.0	354.3	42.7	8	11.1	337.4	-006	79
39.1	35.70759	100.23870	3007	Cir	159.6	-48.7	163.2	-44.1	6	7.6	346.0	163	-73
42.3	35.70781	100.23944	3114	Cir	146.7	-40.5	151.6	-37.8	7	13.1	357.9	152	-62

45	35.70796	100.23941	-	ChR	21.0	59.4	21.0	59.4	5	13.0	425.1	021	73